Intrasteric Inhibition Mediates the Interaction of the I/LWEQ Module Proteins Talin1, Talin2, Hip1, and Hip12 with Actin†

Melissa A. Senetar, Stanley J. Foster, and Richard O. McCann*

Department of Molecular and Cellular Biochemistry, College of Medicine, University of Kentucky, 800 Rose Street, Lexington, Kentucky 40536-0298

Received June 19, 2004; Revised Manuscript Received September 27, 2004

ABSTRACT: The I/LWEQ module superfamily is a class of actin-binding proteins that contains a conserved C-terminal actin-binding element known as the I/LWEQ module. I/LWEQ module proteins include the metazoan talins, the cellular slime mold talin homologues TalA and TalB, fungal Sla2p, and the metazoan Sla2 homologues Hip1 and Hip12 (Hip1R). These proteins possess a similar modular organization that includes an I/LWEQ module at their C-termini and either a FERM domain or an ENTH domain at their N-termini. As a result of this modular organization, I/LWEQ module proteins may serve as linkers between cellular compartments, such as the plasma membrane and the endocytic machinery, and the actin cytoskeleton. Previous studies have shown that I/LWEQ module proteins bind to F-actin. In this report, we have determined the affinity of the I/LWEQ module proteins Talin1, Talin2, huntingtin interacting protein-1 (Hip1), and the Hip1-related protein (Hip1R/Hip12) for F-actin and identified a conserved structural element that interferes with the actin binding capacity of these proteins. Our data support the hypothesis that the actin-binding determinants in native talin and other I/LWEQ module proteins are cryptic and indicate that the actin binding capacities of Talin1, Talin2, Hip1, and Hip12 are regulated by intrasteric occlusion of primary actin-binding determinants within the I/LWEQ module. We have also found that the I/LWEQ module contains a dimerization motif and stabilizes actin filaments against depolymerization. This activity may contribute to the function of talin in cell adhesion and the roles of Hip1, Hip12 (Hip1R), and Sla2p in endocytosis.

The I/LWEQ module was originally identified on the basis of sequence similarity between the C-termini of mouse Talin1 and yeast Sla2p (*1*) and its conserved organization (*2*). It has since been shown to mediate cytoskeletal localization, F-actin binding, and F-actin bundling in a functionally distinct set of proteins (*2*−*5*). The I/LWEQ module is an actin-binding consensus sequence of 186 residues (*4*, *6*) and is found in the focal adhesion protein talin (*7*, *8*), the *Dictyostelium discoideum* talin homologues TalA and TalB (*9*, *10*), fungal Sla2p (*1*), metazoan Hip1 (huntingtin interacting protein-1) (*11*, *12*), and its homologue, Hip12/Hip1R (*3*, *13*). Talin1 serves as the direct connection between ECM-bound integrin receptors and internal focal adhesion components, including actin, vinculin, and focal adhesion kinase (*14*−*16*). Talin2 was identified as an EST[1] from a heart cDNA library (*17*). However, its physiological functions have not been characterized. TalA and TalB are required for chemotaxis and morphogenesis in *D. discoideum* (*9*, *10*). Sla2p is required for the nucleated assembly of actin in yeast (*1*) and binds to clathrin heavy and light chains (*18*). Hip1 was discovered as a binding partner of huntingtin (*12*) and functions in clathrin-mediated endocytosis through binding to adaptor protein-2 and clathrin (*19*). Hip12, which is the human ortholog of mouse Hip1R (*3*), is 47% identical to Hip1 (*13*). Hip12 is a component of clathrin-coated pits (*3*, *20*, *21*). Thus, Sla2p and its metazoan homologues Hip1 and Hip12 may serve as adaptor proteins between the endocytic apparatus and the actin cytoskeleton, just as talin serves as a link between integrins and actin.

The modular structure of I/LWEQ module proteins is diagrammed in Figure 1A. I/LWEQ module proteins containing a FERM domain, which is a linker to the plasma membrane (*22*), include Talin1 and Talin2, and mycetozoan TalA/B. These proteins constitute one principal branch of the I/LWEQ module superfamily (*2*, *4*). The other principal branch of this superfamily consists of fungal Sla2p and metazoan Hip1 and Hip12. Sla2p, Hip1, and Hip12 contain an E/ANTH (epsin or AP180 N-terminal homology) domain, which is required for normal endocytosis and cytoskeletal organization (*23*−*26*). As a function of this conserved architecture, I/LWEQ module proteins are suited to serve as linkers between the actin cytoskeleton and cellular compartments (*4*, *21*).

Several recent studies have demonstrated the importance of I/LWEQ module proteins and the I/LWEQ module itself (*15*, *27*−*30*). For example, Talin1-null fibroblasts exhibit

† This work was supported by grants from the American Heart Association (0365218B) and the American Cancer Society (85-001-13-IRG) to R.O.M. M.A.S. is supported by a predoctoral fellowship from the American Heart Association.

* To whom correspondence should be addressed. E-mail: rmcca1@uky.edu.

[1] Abbreviations: ECM, extracellular matrix; EST, expressed sequence tag; PtdIns (4,5)P_2, phosphatidylinositol 4,5-bisphosphate; USH, upstream α-helix; GST, glutathione *S*-transferase; 3D-PSSM, three-dimensional position-specific scoring matrix; SDS−PAGE, sodium dodecyl sulfate−polyacrylamide gel electrophoresis.

10.1021/bi0487239 CCC: $27.50
Published on Web 11/17/2004

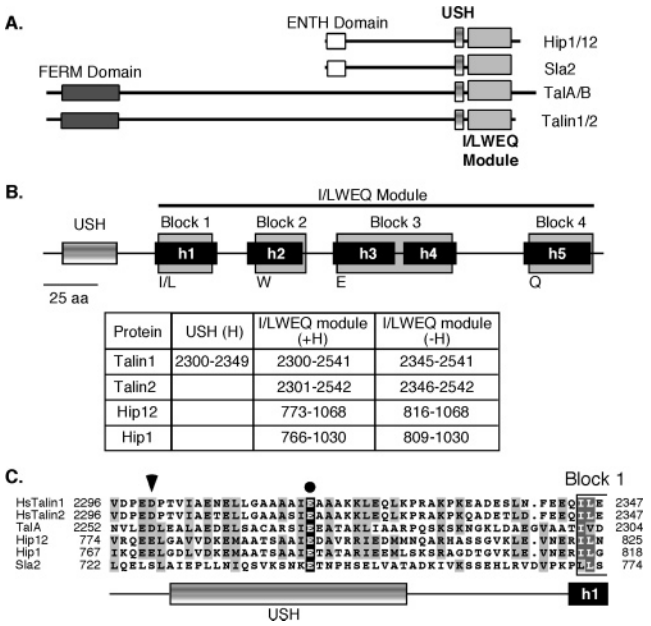

Protein	USH (H)	I/LWEQ module (+H)	I/LWEQ module (-H)
Talin1	2300-2349	2300-2541	2345-2541
Talin2		2301-2542	2346-2542
Hip12		773-1068	816-1068
Hip1		766-1030	809-1030

FIGURE 1: I/LWEQ module superfamily. (A) Representative I/LWEQ module proteins and their similar modular organization. The C-terminal I/LWEQ module, which contains the primary actin-binding site of I/LWEQ module proteins, defines the I/LWEQ module superfamily. The E/ANTH domain of Sla2p, Hip1, and Hip12 (Hip1R) is found in proteins that participate in clathrin-mediated endocytosis. The FERM domain specifies plasma membrane localization in a variety of proteins, including Talin1 and Talin2. (B) Conserved features of the I/LWEQ module. The conserved organization of Blocks 1−4 is shown (gray) along with the putative α-helices (h1−h5, black) that are substantially coextensive with Blocks 1−4. Conserved residues near the beginning of Blocks 1−4 are indicated (I/L, W, E, and Q). The N-terminal, upstream α-helix (USH) is found in all I/LWEQ module proteins (shadowed). The α-helical nature of the I/LWEQ module has been confirmed by circular dichroism spectroscopy. Recombinant I/LWEQ module proteins (±H) and the Talin1 USH are described in the table with reference to their amino acid sequences (GenBank accession numbers O75146 for O75146 and O00291 for O00291; human Talin1 and Talin2 cDNA sequences have been submitted to GenBank). (C) USH sequence alignment. Amino acid sequences N-terminal to the I/LWEQ module of Talin1/2, TalA, Hip1/12, and Sla2p were aligned using CLUSTAL W (*69*). The structurally conserved USH (shadowed) and the beginning of Block 1 of the I/LWEQ module are shown. The first amino acid of the (+H) recombinant proteins is noted with an arrowhead. Conserved amino acids are highlighted in gray. The filled circle and black shading indicate the only invariant amino acid in the USH.

compromised cytoskeletal linkages (*30*). This phenotype can be rescued by expression of full-length Talin1, but expression of a Talin1 mutant lacking the I/LWEQ module results in a phenotype similar to that of the Talin1-null cells (*30*). A temperature-sensitive mutation in yeast *sla2* that essentially eliminated the I/LWEQ module caused defects in endocytosis and cytoskeletal organization similar to those seen in *sla2*-null cells (*1*, *27*, *29*, *31*). RNAi-mediated downregulation of Hip1R (Hip12) revealed that Hip1R is required for the formation of a productive association between the actin cytoskeleton and the endocytic machinery (*28*). Overexpression of a Hip1R truncation mutant that lacked the C-terminal I/LWEQ module caused a phenotype similar to that seen in Hip1R-silenced cells, where cargo-containing clathrin-coated vesicles accumulated at the cell cortex due to delayed or blocked internalization (*28*). These data suggest that I/LWEQ module proteins mediate connections with the actin cytoskeleton, and that the association of these proteins with actin, specifically through the I/LWEQ module, is critical for proper cytoskeletal organization and endocytosis (*4*, *21*).

Secondary structure prediction algorithms predict that the I/LWEQ module consists of five α-helices that are coextensive with Blocks 1−4 (*4*). I/LWEQ module proteins also contain an additional upstream α-helix (USH) that is N-terminal to the I/LWEQ module (Figure 1A,B). Although the USH is not as conserved at the sequence level as the I/LWEQ module, with only one invariant residue compared to 16, it is found in all I/LWEQ module proteins (Figure 1C). Initial experiments aimed at determining whether this structural element affects the actin binding capacity of the I/LWEQ module revealed that inclusion of the USH [Talin1 (+H)] decreased the apparent affinity of I/LWEQ module Talin1 for F-actin *in vitro*. In yeast two-hybrid assays, Sla2p (−H) was shown to interact with actin, while inclusion of the USH region abolished actin binding (*31*). Additional two-hybrid screening revealed a specific interaction between the C-terminus of Sla2p (I/LWEQ module) and a short region N-terminal to the I/LWEQ module (USH) (*31*). Taken together, these findings imply that the C-terminal actin-binding sites of talin, Sla2p, and potentially the entire I/LWEQ module superfamily are cryptic in the native state, and possibly regulated by an intrasteric interaction between the I/LWEQ module and the USH.

Such conformational regulation, in which intramolecular interactions alter the accessibility of functional domains, is widespread among cytoskeletal proteins. Actin-binding determinants and protein−protein interaction domains of vinculin (*32*, *33*), the 34 kDa actin bundling protein from *D. discoideum* (*34*), ezrin (*35*), moesin (*36*), and N-WASP (*37*) are masked in the inactive molecule by an intramolecular association. Upon activation, which is regulated by PtdIns $(4,5)P_2$ in the case of ezrin (*38*, *39*), PtdIns $(4,5)P_2$ and protein−protein interactions in the case of N-WASP (*37*, *40*), or protein−protein interactions for vinculin (*41*), intrasteric inhibition is relieved and functional domains are exposed. For example, vinculin contains an actin-binding site in its C-terminus (*32*, *33*). However, native vinculin does not display a strong affinity for F-actin *in vitro*, because its actin-binding site is masked by an intrasteric interaction with the N-terminus (*33*). This head−tail interaction is specific in *cis* and in *trans* and has been shown to interfere with actin binding (*33*). The binding of talin to vinculin disrupts this interaction and activates vinculin so that it can then interact with F-actin in focal adhesions (*41*).

To further understand I/LWEQ module protein function, we have examined the interactions of I/LWEQ proteins with F-actin. We have determined the relative affinity of the I/LWEQ modules of Talin1, Talin2, Hip1, and Hip12 for muscle (α) and non-muscle ($\beta+\gamma$) F-actin. In addition, we have shown that the USH, which is common to all I/LWEQ module proteins, interferes with the actin binding capacity of these proteins in *cis* and in *trans*. Our data suggest an intrasteric mechanism for the regulation of actin binding in I/LWEQ module proteins *in vivo*, in which the actin binding capacity of Talin1, Talin2, Hip1, and Hip12 is regulated by steric occlusion of primary actin-binding determinants within the I/LWEQ module. Our results also demonstrate that I/LWEQ module proteins are dimers and not only bind to but also stabilize F-actin filaments. This activity may

contribute to the function of I/LWEQ module proteins in multicomponent assemblies such as focal adhesions and the endocytic apparatus.

EXPERIMENTAL PROCEDURES

Protein Preparation. Recombinant hexahistidine and GST fusion proteins were prepared by PCR amplification of the particular coding sequence, recovery of the amplified coding sequence in either pCR2.1 or pCR2.1-TOPO (Invitrogen), and subcloning of the coding sequence into either pET-28c or pET-41c (Novagen). *Escherichia coli* BL21(DE3) cells were used for IPTG-induced protein expression, except for Hip12.816−1068, Hip12.773−1068, Hip1.809−1030, and Hip1.766−1030, which were produced in BL21-CodonPlus (DE3)-RIL cells (Stratagene). Recombinant proteins were purified using standard protocols (*42*). Hexahistidine and GST tags were cleaved with biotinylated thrombin (Novagen) and removed by a combination of affinity and anion-exchange chromatography. Purified proteins were stored at 4 °C in phosphate-buffered saline or buffer A [2 mM Tris (pH 8.0), 0.2 mM $CaCl_2$, 0.2 mM ATP, and 0.5 mM dithiothreitol]. Full-length human Talin1 and Talin2 cDNA sequences prepared by RT-PCR from first-strand cDNA (Origene) were used as PCR templates. A partial human Hip1 cDNA was obtained as an IMAGE clone from Research Genetics. The full-length human Hip12 sequence (KIAA0655) was the generous gift of the Kazusa DNA Research Institute (Chiba, Japan). The production of mouse Talin1.2345−2541, which is identical to the human sequence, has been described (*2*, *4*). GenBank accession numbers for the cDNAs that were used are O75146 for Hip12 and O00291 for Hip1. The following PCR primers were used for other constructs: Talin1.2300−2541, 5′-GACCCTACTGTCATT-3′ and 5′-TTAGTGCTCGTCTCG-3′; Talin1.2300−2349, 5′-GACCCTACTGTCATTG-3′ and 5′-TCAGGCAGCTTCTAGGATTTTGTTCC-3′; Talin2.2346−2542, 5′-ATCTTGGAAGCTGCTAAA-3′ and 5′-TTAGCCCTCATCTTCCCT-3′; Talin2.2301−2542, 5′-GACCCAACTGTCATTGCA-3′ and 5′-TTAGCCCTCATCTTCCCT-3′; Hip12.816−1068, 5′-AAGCTGGAGGTGAACGAG-3′ and 5′-CTAGTAGTTCACGAGTTG-3′; Hip12.773−1068, 5′-GATGTGCGGCAGGAGGAG-3′ and 5′-CTAGTAGTTCACGAGTTG-3′; Hip1.766−1030, 5′-GACATCAAGCAGCAGGAGC-3′ and 5′-CACCATTGGCTTTTTCTTATC-3′; Hip1.809−1030, 5′-GTCAAATTGGAGGTGAATG-3′ and 5′-CACCATTGGCTTTTTCTTATC-3′. Oligonucleotides were obtained from Integrated DNA Technologies. All DNA sequences were confirmed independently by DNA sequence determination prior to protein preparation.

F-Actin Binding. Muscle actin was purified from rabbit skeletal muscle (*43*, *44*) or obtained from Cytoskeleton, Inc. Non-muscle actin, which consisted of a mixture of 80% β-actin and 20% γ-actin, was obtained from Cytoskeleton, Inc. Prior to use in cosedimentation experiments, recombinant I/LWEQ module protein samples were precleared by centrifugation for 20 min at 160000*g* using an S100AT3 rotor in a Sorvall Discovery M120 ultracentrifuge. Protein concentrations were determined following clearance. F-Actin cosedimentation assays were performed in buffer A [2 mM Tris (pH 8.0), 0.2 mM $CaCl_2$, 0.2 mM ATP, and 0.5 mM dithiothreitol], keeping the concentration of the I/LWEQ module protein constant at 2.0 μM while increasing the actin concentration from 0 to 25 μM in a total volume of 50 μL. Actin polymerization was induced by addition of 2 mM $MgCl_2$ and 50 mM KCl and allowed to proceed for 60 min at 22 °C. The critical concentration for actin polymerization is 0.71 μM under these conditions. Following centrifugation at 160000*g* and 22 °C for 20 min, the supernatant and pellet fractions were separated for subsequent analysis with SDS−PAGE using 12% gels. Proteins were visualized by staining with Coomassie Blue G250 or a modified silver stain (*45*, *46*). The stoichiometry of the interaction between I/LWEQ module Talin1 and F-actin was determined in F-actin cosedimentation assays as described previously (*34*), except that the actin concentration was kept constant at 3.0 μM while the I/LWEQ module Talin1 concentration was increased from 0 to 15 μM. The results were analyzed as previously described (*34*).

Data Analysis. I/LWEQ module protein bands from digital images of stained gels were quantified densitometrically using NIH Image version 1.62 (available at http://rsb.info.nih.gov/nih-image/). These data were plotted versus F-actin concentration to represent the actin binding profile of each protein. The percent of recombinant I/LWEQ module protein bound to F-actin was converted to specific binding (SB) as a function of input protein, where SB = (2.0 μM)-(% bound). These data were transformed using GraphPad Prism version 4 (www.graphpad.com) and used to calculate apparent dissociation constants for binding of each protein to F-actin (*47*). Each data point in these analyses was the average of at least two, but not more than four, independent experiments for each protein.

Gel Filtration. I/LWEQ module proteins (±H) were chromatographed on a Sephacryl S-100-HR column (0.7 cm × 48 cm) equilibrated with 10 mM Tris (pH 8.0), 1 mM EDTA, 25 mM KCl, and 0.02% sodium azide. Blue dextran (2000 kDa), bovine serum albumin (67 kDa), ovalbumin (45 kDa), carbonic anhydrase (31 kDa), and cytochrome *c* (13 kDa) were used to calibrate the column. The apparent molecular mass of each I/LWEQ module protein was calculated by plotting the elution volume versus the log of the molecular mass of each calibration protein.

Dynamic Light Scattering. The molecular mass of each I/LWEQ module protein was also determined by dynamic light scattering using a DynaPro99 (ProteinSolutions, Charlottesville, VA). Proteins were dialyzed against phosphate-buffered saline (pH 7.0), filtered twice using a 0.02 μm filter, and analyzed by dynamic light scattering. The instrument was calibrated with bovine serum albumin according to the manufacturer's instructions.

F-Actin Stabilization. F-Actin depolymerization in the presence of I/LWEQ module proteins was assessed using pyrene-labeled rabbit skeletal muscle actin in a fluorescence-based assay (*48*). Rabbit skeletal muscle G-actin (23.5 μM, 61% pyrene-labeled) was polymerized as in the F-actin cosedimentation assays. Actin depolymerization was monitored fluorometrically with a Perkin-Elmer model LS55 luminescence spectrometer (excitation at 365 nm and emission at 407 nm). Depolymerization of F-actin was initiated by diluting pyrene-labeled F-actin to 0.20 μM in a total volume of 250 μL of buffer A. The course of depolymerization was followed for 10 min at 22 °C. The dilution buffer contained either 1.0 μM GST as a negative control or the

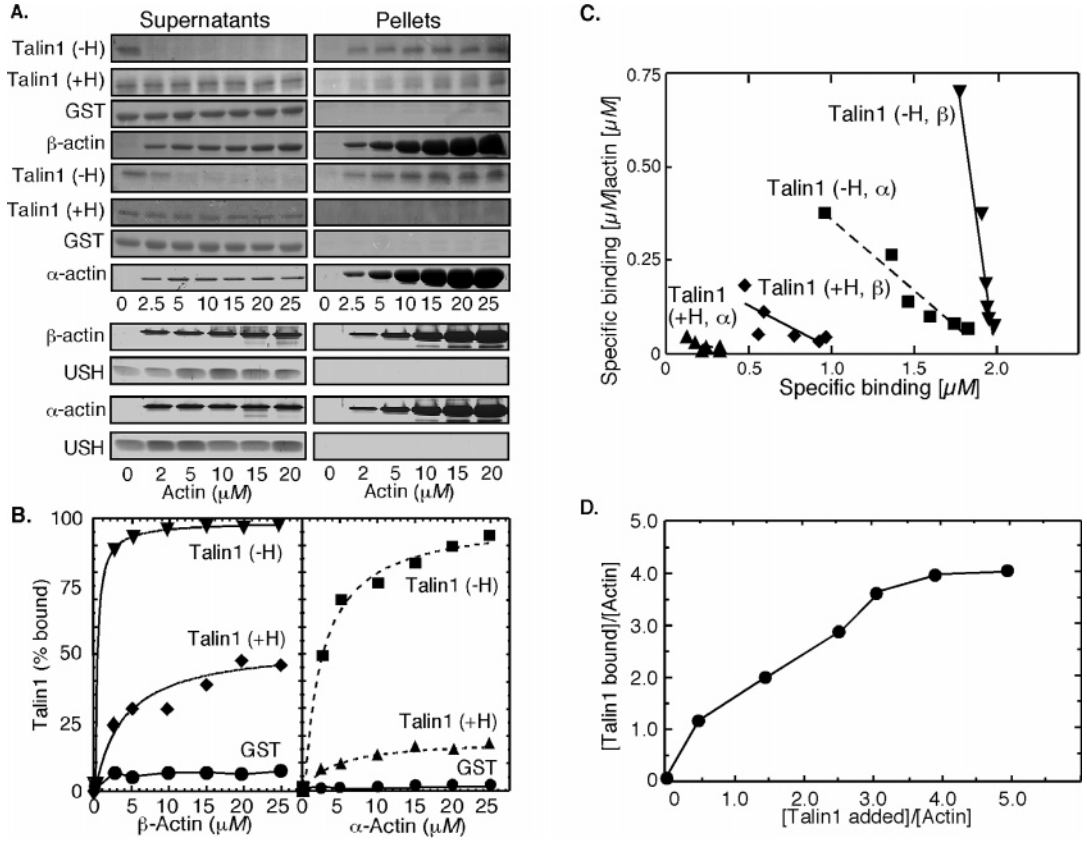

FIGURE 2: Talin1 F-actin binding. (A) F-Actin cosedimentation assays. Muscle (α) or non-muscle (*β*) actin (0−25 *μ*M) was mixed with I/LWEQ module Talin1 (−H), I/LWEQ module Talin1 with the USH (+H), GST, or the Talin1 USH (2.0 *μ*M each) in buffer A [2 mM Tris (pH 8), 0.2 mM $CaCl_2$, 0.2 mM ATP, and 0.5 mM dithiothreitol] in a total volume of 50 *μ*L. Actin polymerization was induced by addition of 2 mM $MgCl_2$ and 50 mM KCl and allowed to proceed for 60 min at 22 °C. Following centrifugation at 160000*g* and 22 °C for 20 min, the supernatant and pellet fractions were separated and F-actin cosedimentation was analyzed by SDS−PAGE. The USH actin binding panels were silver-stained; the others were stained with Coomassie Blue. (B) Quantitative analysis of actin binding. The percent bound, as a measure of cosedimentation of Talin1 (±H) with GST as a negative control, was determined densitometrically using the polyacrylamide gels shown in panel A. The binding data were fit using Kaleidagraph. *R* values for the curve fits ranged from 0.999 to 0.943. (C) Data analysis. Binding curves were transformed and analyzed by linear regression (GraphPad Prism, version 4) to calculate the dissociation constant of Talin1 (±H) for filamentous α- and *β*-actin. Dissociation constants are listed in Table 1. Each data point is the average of at least two but not more than four independent experiments. (D) F-Actin:I/LWEQ module stoichiometry. The stoichiometry for the interaction of the Talin-1 I/LWEQ module and F-actin was determined as described previously (*34*) in cosedimentation assays in which the *β*-actin concentration was kept constant at 3.0 *μ*M while increasing amounts of I/LWEQ module Talin1 (0−15 *μ*M) were added after actin polymerization. The molar ratio of Talin1 to actin was 4.0, indicating that the ratio of Talin1 (+H) dimers to actin was 2:1.

I/LWEQ modules of Talin1, Talin2, Hip1, or Hip12 (all −H) at 1.0 *μ*M.

RESULTS

On the basis of the sequence conservation of I/LWEQ module proteins (*2*, *4*), I/LWEQ-only fusion proteins (−H) were designed to include the initial residue of Block 1 and extend to the C-terminus of Talin1, Talin2, Hip1, and Hip12. I/LWEQ module proteins with the USH (+H) were designed to encode an additional 40−45 residues N-terminal to Block 1 of the I/LWEQ module and extend to the C-terminus of each protein. Thus, all fusion proteins that were used included each of the four conserved Blocks of the I/LWEQ module and differ only in the inclusion or exclusion of the USH (Figure 1).

The cosedimentation of Talin1 (±H) with non-muscle actin is shown in Figure 2A. With an increasing actin concentration, Talin1 (−H) was depleted from the residual supernatant following ultracentrifugation, and this depletion was accompanied by enrichment in the corresponding F-actin pellet fractions. In contrast to Talin1 (−H), only a portion of Talin1 (+H) cosedimented with F-actin (Figure 2A). Neither GST nor the Talin1 USH bound to either actin isoform, and the recombinant Talin1 proteins did not sediment in the absence of F-actin (Figure 2A,B, "0 *μ*M" actin concentration; this was also true for Talin2, Hip1, and Hip12). Cosedimentation of Talin1 (±H) was assessed directly by densitometry as described. Quantitative analysis of the gels shown in Figure 2A is shown in Figure 2B. F-Actin bands serving as internal controls displayed accurate linearity of response for all densitometry measurements (not shown). Calculation of apparent dissociation constants (K_d) for the interaction of Talin1 (±H) with muscle and non-muscle actin by data transformation is shown in Figure 2C, with the K_d values for Talin1 and the other I/LWEQ module proteins listed in Table 1. In addition to measuring the actin binding affinity of Talin1 (−H), we also used Talin1 (−H) to determine the stoichiometry of the interaction between the I/LWEQ module and F-actin (Figure 2D). Talin1 bound to F-actin at a molar ratio of 4:1.

A number of actin-binding proteins, including utrophin and ezrin, display isoform-specific actin binding capacities

Table 1: Dissociation Constants for I/LWEQ Module−F-Actin Interactions[a]

I/LWEQ module	β-actin			α-actin		
	−H	+H	ΔK_d	−H	+H	ΔK_d
Talin1	0.31	4.4	14	2.6	7.5	2.9
Talin2	0.88	1.5	1.7	2.1	3.7	1.8
Hip1	2.5	3.4	1.4	3.0	[14]	nc[b]
Hip12	3.4	[39]	nc[b]	3.3	[29]	nc[b]

[a] Dissociation constants (K_d) were calculated by transforming the binding curves shown in Figures 2 and 3 (transformation illustrated in Figure 2C). The fold change in K_d upon inclusion of the USH is shown as ΔK_d. The decreases in binding affinity range from 1.4-fold for Hip1 with β-actin to 14-fold for Talin1 with β-actin. Values in brackets have been calculated but do not vary significantly from values obtained with GST controls and are therefore not significant. They do, however, illustrate the capacity of the Hip1 and Hip12 USH to essentially abolish the actin binding capacity of their respective I/LWEQ modules in these assays. Values are reported in micromolar. [b] ΔK_d not calculated.

(*49*−*51*). In addition to this variability associated with actin isoforms, proteins that exist as a set of several actin-binding isoforms, such as tropomyosin, bind differentially to F-actin (*52*). Given that our experiments were designed to examine the actin binding capacities of both mammalian isoforms of talin, as well as those of Hip1 and Hip12, we determined the actin binding profiles of these proteins for both muscle (α) and non-muscle (predominantly β) actin isoforms. The data in Figure 2 (A, cosedimentation; B, binding curves; C, K_d calculation) and Table 1 show that Talin1 (−H) bound to β-actin with an 8.4-fold higher affinity than to α-actin (a K_d of 0.31 μM vs a K_d of 2.6 μM). Inclusion of the USH of Talin1 markedly reduced the apparent affinity of I/LWEQ module Talin1 for both α- and β-F-actin [Figure 2A−C, Talin1 (+H)]. The affinity of Talin1 (−H) for β-actin decreased 14-fold upon inclusion of the USH (Table 1, ΔK_d going from 4.4 to 0.31 μM), while the interaction with α-actin showed a 2.9-fold decrease in affinity upon inclusion of the USH (Table 1, ΔK_d going from 7.5 to 2.6 μM).

To determine if the USH is involved in mediating the interaction of other I/LWEQ module proteins and actin, recombinant Talin2, Hip1, and Hip12 (±H) were assayed for interactions with F-actin as shown in Figure 2. The overall behavior of Talin2 (Figure 3A) was similar to that of Talin1, except that the dissociation constants for Talin2 were higher. The apparent K_d of Talin2 (−H) for β-actin was 0.88 μM, which is 2.8-fold higher than the value of 0.31 μM for Talin1 (−H), indicating that Talin2 interacts with actin with a corresponding lower affinity (Table 1). As with the Talin1 I/LWEQ module, Talin2 also had a higher apparent affinity for β-actin than for α-actin (ΔK_d = 2.1 and 0.88 μM, respectively), but the magnitude of the difference was less for Talin2 than for Talin1 (2.4- vs 8.4-fold). As with Talin1, inclusion of the USH reduced the affinity of I/LWEQ module Talin2 (+H) for both β-actin and α-actin (Figure 3A) by 1.7- and 1.8-fold, respectively (Table 1).

Hip1 (−H) has previously been shown to interact with F-actin (*4*), although the actin binding capacity of this I/LWEQ module has been questioned (*20*). Our data show that Hip1 (−H) interacts with F-actin (Figure 3B) with comparable affinities for β-actin and α-actin (K_d = 2.5 and 3.0 μM, respectively; Table 1). However, Hip1 did not interact as strongly with F-actin as Talin1 (−H) or Talin2 (−H). The increase in the dissociation constant was 0.31, 0.88, and 2.5 μM for Talin1, Talin2, and Hip1, respectively, against β-actin. Thus, Talin1 and Talin2 had 8.1- and 2.8-fold higher apparent affinities, respectively, for β-actin than Hip1 (−H). As with Talin1 and Talin2, inclusion of the USH reduced the affinity of I/LWEQ module Hip1 (+H) for β-actin (Figure 3B) by 1.4-fold. However, the USH had a much greater effect on the Hip1-filamentous α-actin interaction, where F-actin binding was essentially abolished upon inclusion of the USH (Figure 3B).

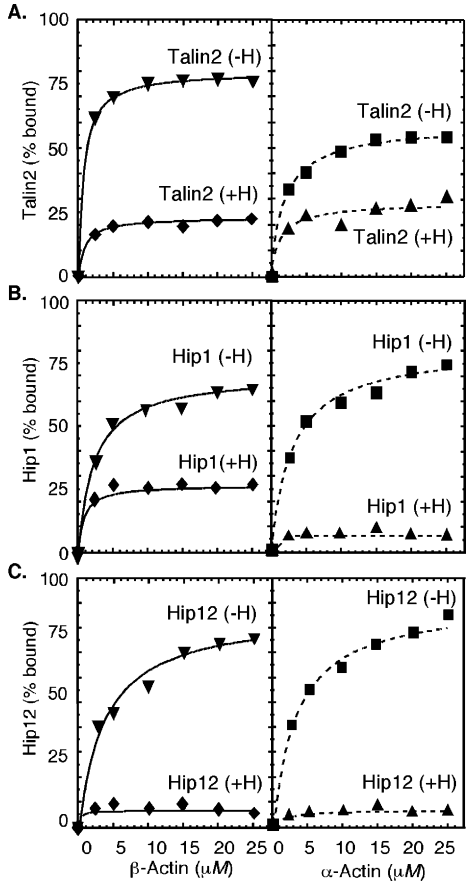

FIGURE 3: Talin2, Hip1, and Hip12 F-actin binding. I/LWEQ module Talin2, Hip1, and Hip12 were analyzed as described in the legend of Figure 2. (A) Talin2 F-actin cosedimentation assays. Talin2 has a lower affinity than Talin1 for both actin isoforms. Inclusion of the USH (+H) decreased the binding affinity for both α- and β-actin. *R* values for the Talin2 curve fits ranged from 0.999 to 0.934. (B) Hip1 F-actin cosedimentation assays. Hip1 has similar binding affinities for both actin isoforms. Inclusion of the USH (+H) decreased the binding affinity for β-actin and essentially abolished the F-actin binding capacity of Hip1 for α-actin. *R* values for the Hip1 curve fits ranged from 0.993 to 0.863. (C) Hip12 F-actin cosedimentation assays. Like Hip1, Hip12 (−H) has similar affinities for both actin isoforms. Inclusion of the USH (+H) abolished the F-actin binding capacity of Hip12 for β- and α-actin. *R* values for the Hip12 curve fits ranged from 0.992 to 0.738. All binding data were transformed as described in the legend of Figure 2 and used to calculate apparent affinity constants. K_d values are listed in Table 1 for comparison. Each data point is the average of at least two but not more than four independent experiments.

Hip12 has previously been shown to interact with F-actin (*20*). Consistent with this observation, we found that Hip12 (−H), like Hip1, exhibited a similar affinity for both β- and α-actin (Figure 3C and Table 1; K_d = 3.4 and 3.3 μM, respectively). I/LWEQ module Talin1 (−H), Talin2 (−H), and Hip1 (−H) have 11-, 3.9-, and 1.4-fold higher apparent affinities for β-actin, respectively, than Hip12 (−H) (Table

1). As with the other three I/LWEQ module proteins, inclusion of the USH reduced the affinity of I/LWEQ module Hip12 (+H) for F-actin. However, in this case, inclusion of the USH abolished the interaction of Hip12 with both α- and β-actin isoforms (Figure 3C).

The data in Figures 2 and 3 and Table 1 demonstrate that the I/LWEQ modules of Talin1, Talin2, Hip1, and Hip12 interact with F-actin and that inclusion of the USH in *cis* interferes with the actin binding capacity of these four I/LWEQ module proteins. Inclusion of the USH has also been shown to interfere with the actin binding capacity of yeast Sla2p in a similar manner (*31*). These observations suggest that an intramolecular interaction between the USH and the I/LWEQ module is responsible for masking the actin-binding site of the I/LWEQ module in these proteins. Such an interaction would be a relatively high-affinity interaction given that (a) the USH caused a 7.5−14-fold reduction in the apparent affinity of the Talin1 I/LWEQ module for both α- and β-F-actin, (b) the USH abolished the interaction of Hip1 with α-F-actin, and (c) the USH abolished the interaction of Hip12 with α- and β-F-actin (Figures 2 and 3 and Table 1). This implies that the USH should be able to act in *trans* to inhibit actin binding as well. Specific competition between functional domains in *trans* has been used to demonstrate that an intramolecular interaction between functional domains inhibits actin binding of both vinculin (*33*) and the 34 kDa F-actin bundling protein from *D. discoideum* (*34*). We used a similar strategy to determine whether the interaction in *cis* of the USH with the I/LWEQ module can be recapitulated in *trans* (Figure 4). F-Actin and Talin1 (−H) were incubated with an increasing concentration of purified USH (Talin1 USH, Figure 1B) and subjected to cosedimentation and densitometry analysis as in Figure 2. With an increase in the concentration of the USH, the amount of Talin1 (−H) bound to F-actin decreased, which is reflected by the decrease in the amount of Talin1 (−H) in the pellet fractions and its concomitant increase in the supernatant (Figure 4A). Quantitative analysis of these data (Figure 4B) showed that, at a 5−10-fold molar excess, the USH inhibited F-actin binding of the Talin1 I/LWEQ module at a level similar to that found with Talin1 (+H) (striped bar; value taken from Figure 2B). Thus, a specific intrasteric interaction between the I/LWEQ module and the USH interferes with the interaction of I/LWEQ module Talin1 with F-actin.

Talin1, Hip1, and Hip12 form dimers *in vitro* and *in vivo* (*13*, *53*, *54*). Using two different techniques, we have found that the I/LWEQ module by itself exists as a dimer in solution. On a gel filtration column, both Talin1 (±H) and Hip1 (+H) eluted at apparent molecular masses consistent with the formation of dimers (Figure 6A,B). Talin1 (−H), which has a calculated molecular mass of 23 038 Da, essentially coeluted with ovalbumin (45 000 Da), for an M_r of 46 000 Da. Talin1 (+H; 26 367 Da) behaved similarly, with an M_r of 52 000 Da on the same column, as did Hip1 (+H; 30 894 Da), which eluted at an elution volume corresponding to 64 000 Da. These results are consistent with the values we have obtained independently for I/LWEQ module proteins using dynamic light scattering (Figure 6C). Using this technique, Talin1 (−H) had an M_r of 45 900 Da, while TalA (+H; 26 482 Da) had an M_r of 51 200 Da. Thus, all I/LWEQ modules behave as dimers in solution.

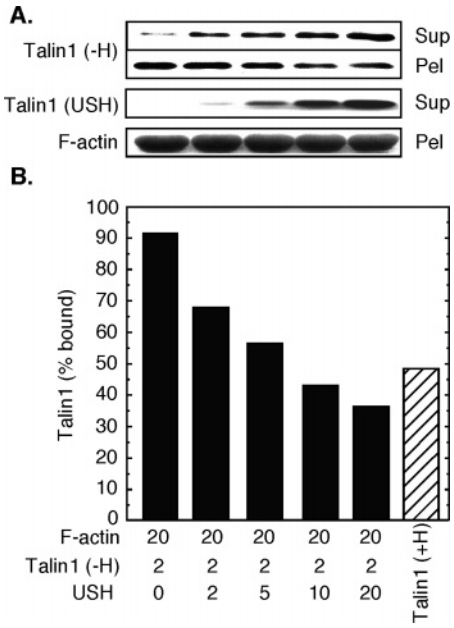

FIGURE 4: Intrasteric inhibition of F-actin binding. (A) SDS−PAGE. α-Actin (20 μM) was mixed with I/LWEQ module Talin1 (−H) and an increasing concentration (0−10 μM) of the Talin1 USH. F-Actin cosedimentation was then carried out as for Figures 2 and 3. F-Actin was visualized with Coomassie Blue staining; the Talin1 USH was visualized by silver staining, while Talin1 (−H) was detected by immunoblotting. (B) Quantitative analysis. The percent bound, as a measure of the extent of cosedimentation of I/LWEQ module Talin1 in the presence of increasing amounts of Talin1 USH in *trans* (−H, black bars), was determined densitometrically using the data shown in panel A. Increasing the amount of the USH decreased the actin binding level of I/LWEQ module Talin1. The Talin1 (+H) value (striped bar) is taken from Figure 2B to show that the *trans* I/LWEQ module−USH interaction mimics the *cis* interaction. Values are averages of two separate experiments.

DISCUSSION

We have examined the actin binding capacity of representative I/LWEQ module proteins using F-actin cosedimentation assays with both muscle and non-muscle actin. We have shown that I/LWEQ module proteins bind differentially to these actin isoforms. We have also demonstrated that a conserved structural element N-terminal to the I/LWEQ module (USH) interferes with the intrinsic actin binding capacity of these proteins. These results indicate that the interactions between I/LWEQ module proteins and actin are subject to intrasteric regulation in a manner similar to that found with other actin-binding proteins. We have also found that the I/LWEQ module contains a dimerization motif, which may contribute to the function of these proteins *in vivo*.

Actin Binding and Isoform Specificity. Analysis of the actin binding capacity of I/LWEQ module Talin1, Talin2, Hip1, and Hip12 with non-muscle and muscle actin revealed that I/LWEQ module Talin1 (−H) has the highest relative affinity for β-actin, followed by Talin2, Hip1, and Hip12 (Table 1). In our assays, I/LWEQ module Talin2 (−H) exhibits the highest relative affinity for α-actin, followed by Hip12, Talin1, and Hip1 (Table 1), although, in general, each of these proteins interacts with α-actin with a lower affinity than with β-actin. The isoform specificity of these interactions may have functional significance. For example, the interaction of Talin1 (−H) with β-actin is 8.4-fold stronger

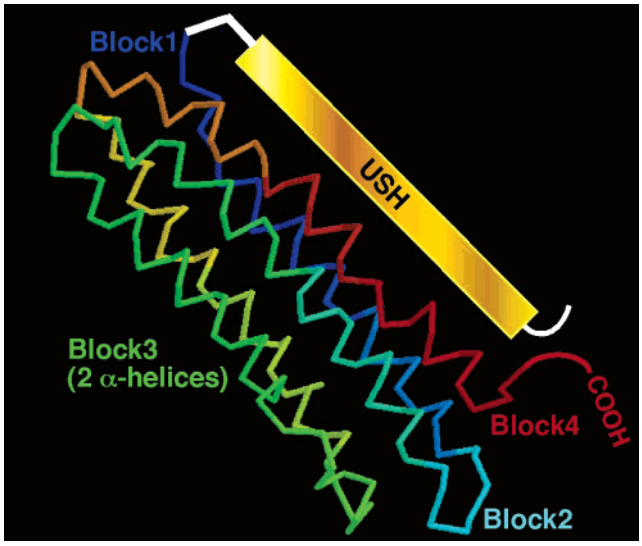

FIGURE 5: Model of intrasteric inhibition for I/LWEQ module proteins. I/LWEQ module Talin1 (+H) was used as a query sequence against the 3D-PSSM web server, version 2.6.0 (*65*). The I/LWEQ module Talin1 sequence profile and secondary structure prediction were then scanned against the 3D-PSSM fold library to identify structural matches. The coordinates of the top 3D-PSSM match, apolipophorin iii ($E = 0.523$), served as a template for the Talin1 I/LWEQ module sequence to be aligned. Although the E value for this prediction is high, our data support a model in which the USH, by being in close apposition to Block 4 (red), may interfere with the interaction of the I/LWEQ module with F-actin. This model was analyzed using RasMac.

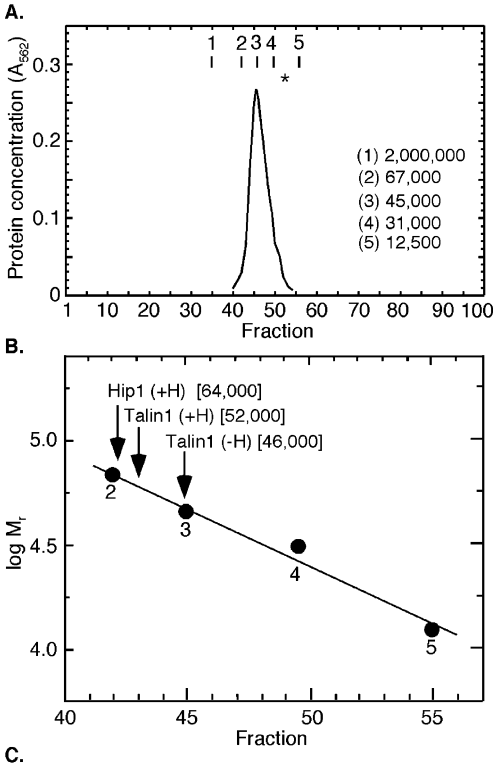

C.

	Calculated Monomer	Calculated Dimer	Dynamic Light Scattering
Talin1 (-H)	23,028	46,056	45,900
TalA (+H)	26,482	52,964	51,200

FIGURE 6: I/LWEQ module protein dimerization. (A) Gel filtration. Talin1 (−H) has a calculated molecular mass of 23 028 Da but essentially coelutes with ovalbumin (M_r = 45 000 Da) on a Sephacryl-S100-HR column, indicating that the protein behaves as a dimer in solution. The predicted elution volume of monomeric Talin1 (−H) is marked with an asterisk. The elution volumes and molecular mass of the calibration standards are indicated. Talin1 (−H) was detected (A_{562}) using the BCA protein assay (Pierce). (B) Calculation of the apparent molecular mass. Talin-1 (+H, 26 367 Da) and Hip1 (+H, 30 894 Da) were also chromataographed on the Sephacryl-S100-HR column. These results are shown here on a plot of log M_r vs elution volume. As with Talin1 (−H), both Talin1 (+H) and Hip1 (+H) eluted as dimers: Talin1 (+H) at 52 000 Da and Hip1 (+H) at 64 000 Da. (C) Dynamic light scattering. The molecular masses of Talin1 (−H) and TalA (+H) were determined using dynamic light scattering. Both proteins had molecular masses corresponding to dimers. As with the gel filtration data, dimerization was independent of the presence of the USH.

than the interaction with α-actin (Table 1). However, the difference for Talin2 (−H) is smaller, with an only 2.4-fold difference. These differences may reflect that the physiological roles of Talin1 and Talin2 are coupled to the well-characterized, distinct cellular roles of actin isoforms.

Several other actin-binding proteins behave in a manner similar to that of Talin1 and Talin2 with respect to their actin binding properties. For example, utrophin is a membrane-associated linker protein required for the maturation of vertebrate neuromuscular junctions (*55*). In cosedimentation assays similar to those used here, the utrophin actin-binding domain bound more tightly to β-actin than to α-actin (*49*). The FERM domain protein ezrin has also been shown to bind preferentially to β-actin (*50*, *51*).

Although actin is a highly conserved protein (*56*), the actin isoforms are generally accepted to have different cellular functions (*57*). Several studies have shown that actin isoforms are sorted independently into distinct subcellular regions (*57*−*59*). The colocalization of actin-binding proteins with specific actin isoforms may reflect the physiological functions of both the actin-binding protein and actin. For example, Talin1, which has the highest relative affinity for non-muscle actin, may be the primary talin isoform found in focal adhesions where β-actin is also enriched (*57*, *60*−*63*).

USH and Steric Inhibition of Actin Binding. Inclusion of the USH yielded a pronounced reduction in the affinity of Talin1, Talin2, Hip1, and Hip12 for both non-muscle and muscle actin (Figures 2 and 3 and Table 1). The importance of the protein sequence upstream of the I/LWEQ module has also been observed for yeast Sla2p. Recombinant Sla2.768−968, which corresponds to Sla2p (−H), interacts with actin in a yeast two-hybrid assay. However, Sla2.503−968, which includes the inhibitory USH, does not interact with F-actin (*31*). These data for Sla2p agree with our results for Talin1, Talin2, Hip1, and Hip12. Similar results have been obtained for Sla2p and TalA (not shown) in F-actin cosedimentation assays. Our data are also in agreement with previous results obtained for Hip12 (*20*). However, previous studies have suggested that Hip1 does not interact with α-F-actin (*20*). The Hip1 construct (Hip1.731−1030) used in that study corresponds to the Hip1 (+H) construct (Hip1.766−1030) we have used here (Figures 1 and 3). This apparent conflict with our results can be easily reconciled given that inclusion of the USH abolishes the interaction of Hip1 with filamentous α-actin (Figure 3 and Table 1).

The inhibition of actin binding implies that the USH interacts with, and subsequently masks, the actin-binding determinants of the I/LWEQ module in an intramolecular interaction between the USH and the I/LWEQ module. The

likely importance of this interaction *in vivo* is illustrated by the phenotype of Chinese hamster ovary cells expressing high levels of a GFP−Talin1 (−H) construct (*4*). These cells exhibit grossly dysregulated actin filaments, probably due to the capacity of the exposed I/LWEQ module to cross-link actin filaments (*2*). This indicates that the USH−I/LWEQ module interaction must be relieved *in vivo* before a strong interaction between actin and the I/LWEQ module can be established.

Our data show that the regulation of I/LWEQ module proteins may be similar to that of other cytoskeleton-associated proteins whose interactions with the actin cytoskeleton are regulated by intrasteric mechanisms. These include the 34 kDa actin bundling protein from *D. discoideum* (*34*), vinculin (*32*, *33*), moesin (*36*), ezrin (*35*), and N-WASP (*64*). In the case of vinculin, the head−tail intrasteric interaction that interferes with actin binding *in vitro* was confirmed by showing that the vinculin head and tail domains interact in *cis* as well as in *trans* (*33*). We used a similar approach to show that the USH of Talin1 also interferes with the interaction of the Talin1 I/LWEQ module with F-actin in *trans* (Figure 4). Incubation of I/LWEQ module Talin1 (−H) with an increasing concentration of the Talin1 USH inhibited the I/LWEQ module−actin interaction (Figure 4). In this experiment, the tight association between Talin1 (−H) and F-actin illustrated in Figure 2 was weakened by the USH. These data parallel the actin binding profile of Talin1 (+H) (compare Figures 2B and 4B). Recapitulation of the USH−I/LWEQ module interaction in *trans* indicates that the USH−I/LWEQ module interaction is specific. Interestingly, the diminished actin binding capacity of Talin1 (+H) mimics that of native talin *in vitro*. Retrospective calculation of the K_d of native chicken gizzard talin (isoform composition unknown) yields a value of 7.0 μM for α-actin (*2*). This agrees well with the K_d of 7.5−3.7 μM for I/LWEQ module Talin1 and Talin2 versus α-actin (Table 1). Thus, our results show that the specific intrasteric interaction between the USH and the I/LWEQ module may be responsible for the comparatively weak actin binding capacity of native talin *in vitro*. Our data also agree with previous studies on yeast Sla2p, which demonstrated a specific interaction between the C-terminus of Sla2p (I/LWEQ module) and a short region N-terminal to the I/LWEQ module (USH). As with Talin1, this intrasteric interaction is directly responsible for the inhibition of actin binding of Sla2p (*31*).

We have observed this intrasteric inhibition in representatives of both branches of the I/LWEQ module superfamily (Figure 1) (*2*, *4*), which suggests that the USH−I/LWEQ module interaction has been conserved. Block 4 of the I/LWEQ module contains two highly conserved arginine residues, R2519 and R2526 for Talin1 (*4*). R2526 is required for actin binding (*2*, *4*), but the function of R2519 is unknown. Each USH of Talin1, Talin2, Hip1, Hip12, and Sla2p contains an invariant glutamate residue near the center of the USH, represented by E2317 in Talin1 (Figure 1C). We hypothesize that the USH may interact directly with Block 4 of the I/LWEQ module through an electrostatic interaction between these conserved, oppositely charged residues. To further understand this intramolecular interaction, we have modeled the structure of I/LWEQ module Talin1 (−H) using 3D-PSSM (*65*). The predicted five-helix bundle tertiary structure (Figure 5) corresponds with the secondary structure of I/LWEQ module proteins (*2*, *4*) (Figure 1B). Most interestingly, the USH can be modeled in close apposition to Block 4. Thus, this model structure is consistent with our biochemical data showing that the USH blocks the actin-binding site of the I/LWEQ module. The mechanism of this intrasteric regulation remains to be determined. The conformational activation of ERM proteins is a sequential process triggered through interactions with PtdIns (4,5)P_2 and subsequent phosphorylation of a conserved residue at the interface of the domains involved in intrasteric inhibition (*36*, *39*, *66*). Relief of the USH−I/LWEQ module interaction may be regulated in a similar fashion. For example, the conformation of Talin1 is dependent on PtdIns (4,5)P_2 binding (*67*). Phosphoinositides are also involved in clathrin-coated vesicle formation (*26*). Therefore, the conformation of Hip1 and Hip12 may also be dependent on PtdIns (4,5)P_2. Alternatively, post-translational modifications or specific protein−protein interactions found in the multiprotein assemblies (e.g., focal adhesions and clathrin-coated pits) in which I/LWEQ module proteins are found may be involved in exposing the actin-binding site of the I/LWEQ module, perhaps by interacting directly with the USH or by the altering the interface between the USH and the I/LWEQ module.

I/LWEQ Module Dimerization. The close correspondence of the elution volume with calculated molecular mass as dimers indicates that the I/LWEQ modules of Talin1 and Hip1 form homodimers that are globular in conformation. Using Talin1 (−H) as an exemplar of the superfamily, we found that the I/LWEQ module binds to F-actin at a molar ratio of 4:1 (Figure 2D). Since the I/LWEQ module constructs used in this study dimerize *in vitro* (Figure 6A−C), the molar ratio of the functional, dimeric I/LWEQ module protein to actin is 2:1. This dimerization may account for the ability of the I/LWEQ module to cross-link actin filaments *in vitro* (*2*). Interestingly, dimerization is independent of the presence of the USH, as both Talin1 (+H) and Talin1 (−H) exist as dimers in solution (Figure 6). Therefore, dimerization and actin binding are separable elements within the I/LWEQ module, because actin binding, but not dimerization, is affected by the USH. Talin1, Hip1, and Sla2 form homodimers *in vivo*. As Hip1 (+H) and Talin1 (±H) form dimers, the I/LWEQ module may be the primary actin-binding site and the dimerization motif for these proteins. Hip1 and Hip12 also form a heterodimeric complex (*13*). This implies that the USH of one protein may interact with the I/LWEQ module of the other in the regulation of actin binding. Studies aimed at determining the relationship between I/LWEQ module dimerization and the regulation of actin binding are currently underway.

Actin Filament Stabilization and I/LWEQ Module Proteins in Endocytosis. The involvement of the actin cytoskeleton in endocytosis is widely accepted but still not completely understood (*68*). Downregulation of Hip1R (Hip12) in mammalian cells or deletion of Sla2p in yeast cells causes an arrest of endocytosis at the internalization step, concomitant with the formation of actin comet tails at the unproductive endocytic site at the plasma membrane (*1*, *28*, *31*). These results confirm that I/LWEQ module proteins are involved in endocytosis in both yeast and animal cells, where these actin-binding proteins may mediate the association of the actin cytoskeleton and the endocytic apparatus and be

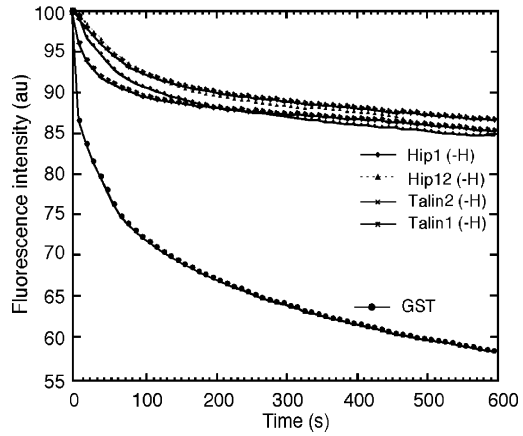

FIGURE 7: Stabilization of F-actin by the I/LWEQ module. F-Actin (23.5 μM, 61% pyrene-labeled) was depolymerized in the presence of GST or a 5-fold molar excess of each I/LWEQ module (1 μM each). F-Actin depolymerization was initiated by dilution to 0.20 μM F-actin in buffer A and monitored by the decrease in pyrene fluorescence. All I/LWEQ module proteins that were tested stabilized F-actin against depolymerization relative to the GST negative control.

responsible for a functional association between the two. Abnormal actin comet tails containing short, misshapen actin filaments and unproductive, arrested endocytic complexes are observed in the presence of both yeast Sla2p and mammalian Hip1R (Hip12) mutants lacking the I/LWEQ module (*27*, *28*). These data suggest that Sla2p and Hip12 mediate endocytosis through the I/LWEQ module and that the association between actin and the endocytic machinery is crucial for internalization and productive endocytosis.

Stable actin filaments are required for the completion of the early, plasma membrane-proximal steps of endocytosis (*29*). We have found that the I/LWEQ modules of the four proteins used in this study stabilize F-actin polymers against depolymerization *in vitro* (Figure 7). Because these proteins function as dimers *in vivo*, F-actin stability may be induced by cross-linking of actin filaments. The ability of the I/LWEQ module to stabilize actin filaments may account for the requirement of a functional Sla2p or Hip1R in endocytosis and could explain why actin filaments are so short and tightly wound in the Hip1R knockdowns in mammalian cells and in the yeast *sla2* mutants lacking the I/LWEQ module (*27*−*29*). That both Sla2p and Hip12 (Hip1R) stabilize actin filaments, while linking the endocytic apparatus to the actin cytoskeleton, implies that these two physiological functions of I/LWEQ module proteins are essential for endocytosis.

The data presented here provide direct evidence that I/LWEQ module proteins not only bind to but also stabilize F-actin filaments. We have shown that a specific, intramolecular interaction between the USH and I/LWEQ module is conserved across the I/LWEQ module superfamily, and our findings suggest that I/LWEQ module−actin interactions are regulated *in vivo* by modulation of the USH−I/LWEQ module interaction. This masking and unmasking of the actin-binding sites of the I/LWEQ module may contribute to the recruitment of I/LWEQ module proteins in the assembly and functionality of focal adhesions and the endocytic machinery. Further molecular and structural characterization of the I/LWEQ module−USH interaction will improve our understanding of the regulation and function of these ancient, conserved proteins as components of complex multiprotein assemblies involved in cell motility and adhesion and in vesicle trafficking during endocytosis.

ACKNOWLEDGMENT

We thank Kazusa DNA Research for providing the human Hip12 cDNA (KIAA0655), David Rodgers for help with dynamic light scattering, and Carole L. Moncman and Thomas C. Vanaman for technical advice and reading the manuscript.

REFERENCES

1. Holtzman, D. A., Yang, S., and Drubin, D. G. (1993) Synthetic-lethal interactions identify two novel genes, *SLA1* and *SLA2*, that control membrane cytoskeleton assembly in *Saccharomyces cerevisiae*, *J. Cell Biol. 122*, 635−644.
2. McCann, R. O., and Craig, S. W. (1997) The I/LWEQ module: A conserved sequence that signifies F-actin binding in functionally diverse proteins from yeast to mammals, *Proc. Natl. Acad. Sci. U.S.A. 94*, 5679−5684.
3. Engqvist-Goldstein, A. E., Kessels, M. M., Chopra, V. S., Hayden, M. R., and Drubin, D. G. (1999) An actin-binding protein of the Sla2/Huntingtin interacting protein-1 family is a novel component of clathrin-coated pits and vesicles, *J. Cell Biol. 147*, 1503−1518.
4. McCann, R. O., and Craig, S. W. (1999) Functional genomic analysis reveals the utility of the I/LWEQ module as a predictor of protein:actin interaction, *Biochem. Biophys. Res. Commun. 266*, 135−140.
5. Tremuth, L., Kreis, S., Melchior, C., Hoebeke, J., Ronde, P., Plancon, S., Takeda, K., and Kieffer, N. (2004) A fluorescence cell biology approach to map the second integrin-binding site of talin to a 130 amino acid sequence with the rod domain, *J. Biol. Chem. 279*, 22258−22266.
6. Bateman, A., Birney, E., Durbin, R., Eddy, S. R., Howe, K. L., and Sonnhammer, E. L. (2000) The Pfam protein families database, *Nucleic Acids Res. 28*, 263−266.
7. Burridge, K., and Connell, L. (1983) A new protein of adhesion plaques and ruffling membranes, *J. Cell Biol. 97*, 359−367.
8. Rees, D. J., Ades, S. E., Singer, S. J., and Hynes, R. O. (1990) Sequence and domain structure of talin, *Nature 347*, 685−689.
9. Kreitmeier, M., Gerisch, G., Heizer, C., and Muller-Taubenberger, A. (1995) A talin homologue of *Dictyostelium* rapidly assembles at the leading edge of cells in response to chemoattractant, *J. Cell Biol. 129*, 179−188.
10. Tsujioka, M., Machesky, L. M., Cole, S. L., Yahata, K., and Inouye, K. (1999) A unique talin homologue with a villin headpiece-like domain is required for multicellular morphogenesis in *Dictyostelium*, *Curr. Biol. 9*, 389−392.
11. Kalchman, M. A., Koide, H. B., McCutcheon, K., Graham, R. K., Nichol, K., Nishiyama, K., Kazemi-Esfarjani, P., Lynn, F. C., Wellington, C., Metzler, M., Goldberg, Y. P., Kanazawa, I., Gietz, R. D., and Hayden, M. R. (1997) HIP1, a human homologue of *S. cerevisiae* Sla2p, interacts with membrane-associated huntingtin in the brain, *Nat. Genet. 16*, 44−53.
12. Wanker, E. E., Rovira, C., Scherzinger, E., Hasenbank, R., Walter, S., Tait, D., Colicelli, J., and Lehrach, H. (1997) HIP-I: A huntingtin interacting protein isolated by the yeast two-hybrid system, *Hum. Mol. Genet. 6*, 487−495.
13. Chopra, V. S., Metzler, M., Rasper, D. M., Engqvist-Goldstein, A. E., Singaraja, R., Gan, L., Fichter, K. M., McCutcheon, K., Drubin, D., Nicholson, D. W., and Hayden, M. R. (2000) HIP12 is a non-proapoptotic member of a gene family including HIP1, an interacting protein with huntingtin, *Mamm. Genome 11*, 1006−1015.
14. Giancotti, F. G. (2000) Complexity and specificity of integrin signaling, *Nat. Cell Biol. 2*, E13−E14.
15. Calderwood, D. A., and Ginsberg, M. H. (2003) Talin forges the link between integrins and actin, *Nat. Cell Biol. 5*, 694−697.
16. Nayal, A., Webb, D. J., and Horwitz, A. (2004) Talin: An emerging focal point of adhesion dynamics, *Curr. Opin. Cell Biol. 16*, 94−98.
17. McCann, R. O., and Craig, S. W. (1998) Identification of a novel isoform of the focal adhesion protein talin, *Mol. Biol. Cell 9* (Suppl S.), 798.

18. Henry, K. R., D'Hondt, K., Chang, J., Newpher, T., Huang, K., Hudson, R. T., Riezman, H., and Lemmon, S. K. (2002) Scd5p and clathrin function are important for cortical actin organization, endocytosis, and localization of Sla2p in yeast, *Mol. Biol. Cell 13*, 2607−2625.
19. Metzler, M., Legendre-Guillemin, V., Gan, L., Chopra, V., Kwok, A., McPherson, P. S., and Hayden, M. R. (2001) HIP1 functions in clathrin-mediated endocytosis through binding to clathrin and adaptor protein 2, *J. Biol. Chem. 276*, 39271−39276.
20. Legendre-Guillemin, V., Metzler, M., Charboneau, M., Gan, L., Chopra, V., Philie, J., Hayden, M. R., and McPherson, P. S. (2002) Hip1 and Hip12 display differential binding to F-actin, AP2, and clathrin. Identification of a novel interaction with clathrin light chain, *J. Biol. Chem. 277*, 19897−19904.
21. Engqvist-Goldstein, A. E., and Drubin, D. (2003) Actin assembly and endocytosis: From yeast to mammals, *Annu. Rev. Cell Dev. Biol. 19*, 287−332.
22. Chishti, A. H., Kim, A. C., Marfatia, S. M., Lutchman, M., Hanspal, M., Jindal, H., Liu, S. C., Low, P. S., Rouleau, G. A., Mohandas, N., Chasis, J. A., Conboy, J. G., Gascard, P., Takakuwa, Y., Huang, S. C., Benz, E. J., Jr., Bretscher, A., Fehon, R. G., Gusella, J. F., Ramesh, V., Solomon, F., Marchesi, V. T., Tsukita, S., Hoover, K. B., et al. (1998) The FERM domain: A unique module involved in the linkage of cytoplasmic proteins to the membrane, *Trends Biochem. Sci. 23*, 281−282.
23. Kay, B. K., Yamabhai, M., Wendland, B., and Emr, S. D. (1999) Identification of a novel domain shared by putative components of the endocytic and cytoskeletal machinery, *Protein Sci. 8*, 435−438.
24. Rosenthal, J. A., Chen, H., Slepnev, V. I., Pellegrini, L., Salcini, A. E., Di Fiore, P. P., and De Camilli, P. (1999) The epsins define a family of proteins that interact with components of the clathrin coat and contain a new protein module, *J. Biol. Chem. 274*, 33959−33965.
25. Wendland, B., Steece, K. E., and Emr, S. D. (1999) Yeast epsins contain an essential N-terminal ENTH domain, bind clathrin and are required for endocytosis, *EMBO J. 18*, 4383−4393.
26. Legendre-Guillemin, V., Wasiak, S., Hussain, N. K., Angers, A., and McPherson, P. S. (2004) ENTH/ANTH proteins and clathrin-mediated membrane budding, *J. Cell Sci. 117*, 9−18.
27. Baggett, J. J., D'Aquion, K. E., and Wendland, B. (2003) The Sla2p talin domain plays a role in endocytosis in *Saccharomyces cerevisiae*, *Genetics 165*, 1661−1674.
28. Engqvist-Goldstein, A. E., Zhang, C. X., Carreno, S., Barroso, C., Heuser, J. E., and Drubin, D. (2004) RNAi-meidated Hip1R silencing results in stable association between the endocytic machinery and the actin assembly machinery, *Mol. Biol. Cell 15*, 1666−1679.
29. Kaksonen, M., Sun, Y., and Drubin, D. G. (2003) A pathway for association of receptors, adaptors, and actin during endocytic internalization, *Cell 115*, 475−487.
30. Jiang, G., Giannone, G., Critchley, D. R., Fukumoto, E., and Sheetz, M. P. (2003) Two-piconewton slip bond between fibronectin and the cytoskeleton depends on talin, *Nature 424*, 334−337.
31. Yang, S., Cope, M. J., and Drubin, D. G. (1999) Sla2p is associated with the yeast cortical actin cytoskeleton via redundant localization signals, *Mol. Biol. Cell 10*, 2265−2283.
32. Johnson, R. P., and Craig, S. W. (1994) An intramolecular association between the head and tail domains of vinculin modulates talin binding, *J. Biol. Chem. 269*, 12611−12619.
33. Johnson, R. P., and Craig, S. W. (1995) F-Actin binding site masked by the intramolecular association of vinculin head and tail domains, *Nature 373*, 261−264.
34. Lim, R. W., Furukawa, R., and Fechheimer, M. (1999) Evidence of intramolecular regulation of the *Dictyostelium discoideum* 34,000 Da F-actin-bundling protein, *Biochemistry 38*, 16323−16332.
35. Gary, R., and Bretscher, A. (1995) Ezrin self-association involves binding of an N-terminal domain to a normally masked C-terminal domain that includes the F-actin binding site, *Mol. Biol. Cell 6*, 1061−1075.
36. Pearson, M. A., Reczek, D., Bretscher, A., and Karplus, P. A. (2000) Structure of the ERM protein moesin reveals the FERM domain fold masked by an extended actin binding tail domain, *Cell 101*, 259−270.
37. Rohatgi, R., Ho, H. Y., and Kirschner, M. W. (2000) Mechanism of N-WASP activation by CDC42 and phosphatidylinositol 4,5-bisphosphate, *J. Cell Biol. 150*, 1299−1310.
38. Sechi, A. S., and Wehland, J. (2000) The actin cytoskeleton and plasma membrane connection: PtdIns(4,5)P(2) influences cytoskeletal protein activity at the plasma membrane, *J. Cell Sci. 113*, 3685−3695.
39. Fievet, B. T., Gautreau, A., Roy, C., Del Maestro, L., Mangeat, P., Louvard, D., and Arpin, M. (2004) Phosphoinositide binding and phosphorylation act sequentially in the activation mechanism of ezrin, *J. Cell Biol. 164*, 653−659.
40. Hussain, N. K., Jenna, S., Glogauer, M., Quinn, C. C., Wasiak, S., Guipponi, M., Antonarakis, S. E., Kay, B. K., Stossel, T. P., Lamarche-Vane, N., and McPherson, P. S. (2001) Endocytic protein intersectin-l regulates actin assembly via Cdc42 and N-WASP, *Nat. Cell Biol. 3*, 927−932.
41. Izard, T., Evans, G., Borgon, R. A., Rush, C. L., Bricogne, G., and Bois, P. R. J. (2004) Vinculin activation by talin through helical bundle conversion, *Nature 427*, 171−175.
42. Golemis, E. (2002) *Protein−Protein Interactions*, Cold Spring Harbor Laboratory Press, Plainview, NY.
43. MacLean-Fletcher, S., and Pollard, T. D. (1980) Identification of a factor in conventional muscle actin preparations which inhibits actin filament self-association, *Biochem. Biophys. Res. Commun. 96*, 18−27.
44. Spudich, J. A., and Watt, S. (1971) The regulation of rabbit skeletal muscle contraction. I. Biochemical studies of the interaction of the tropomyosin-troponin complex with actin and the proteolytic fragments of myosin, *J. Biol. Chem. 246*, 4866−4871.
45. Merril, C. R., Goldman, D., Sedman, S. A., and Ebert, M. H. (1981) Ultrasensitive stain for proteins in polyacrylamide gels shows regional variation in cerebrospinal fluid proteins, *Science 211*, 1437−1438.
46. Morrissey, J. H. (1981) Silver stain for proteins in polyacrylamide gels: A modified procedure with uniform sensitivity, *Anal. Biochem. 117*, 307−310.
47. Schell, M. J., C., E., and Irvine, R. F. (2001) Inositol 1,4,5-triphosphate 3-kinase A associates with F-actin and dendritic spines via its N-terminus, *J. Biol. Chem. 276*, 37537−37546.
48. Cooper, J. A., Walker, S. B., and Pollard, T. D. (1983) Pyrene actin: Documentation of the validity of a sensitive assay for actin polymerization, *J. Muscle Res. Cell Motil. 4*, 253−262.
49. Moores, C. A., and Kendrick-Jones, J. (2000) Biochemical characterisation of the actin-binding properties of utrophin, *Cell Motil. Cytoskel. 46*, 116−128.
50. Shushter, C. B., and Herman, I. M. (1995) Indirect association of ezrin with F-actin: Isoform specificity and calcium sensitivity, *J. Cell Biol. 128*, 837−848.
51. Yao, X., Cheng, L., and Forte, J. G. (1996) Biochemical characterization of ezrin-actin interaction, *J. Biol. Chem. 271*, 7224−7229.
52. Gunning, P., Weinberger, R., and Jeffrey, P. (1997) Actin and tropomyosin isoforms in morphogenesis, *Anat. Embryol. 195*, 311−315.
53. Goldmann, W. H., Bremer, A., Haner, M., Aebi, U., and Isenberg, G. (1994) Native talin is a dumbbell-shaped homodimer when it interacts with actin, *J. Struct. Biol. 112*, 3−10.
54. Wesp, A., Hicke, L., Palecek, J., Lombardi, R., Aust, T., Munn, A. L., and Riezman, H. (1997) End4p/Sla2p interacts with actin-associated proteins for endocytosis in *Saccharomyces cerevisiae*, *Mol. Biol. Cell 8*, 2291−2306.
55. Deconinck, A. E., Potter, A. C., Tinsley, J. M., Wood, S. J., Vater, R., Young, C., Metzinger, L., Vincent, A., Slater, C. R., and Davies, K. E. (1997) Postsynaptic abnormalities at the neuromuscular junctions of utrophin-deficient mice, *J. Cell Biol. 136*, 883−894.
56. Vandekerckhove, J., and Weber, K. (1979) The complete amino acid sequence of actins from bovine aorta, bovine heart, bovine fast skeletal muscle, and rabbit slow skeletal muscle. A protein-chemical analysis of muscle actin differentiation, *Differentiation 14*, 123−133.
57. Khaitlina, S. Y. (2001) Functional specificity of actin isoforms, *Int. Rev. Cytol. 202*, 35−98.
58. Bassell, G., and Singer, R. H. (1997) mRNA and cytoskeletal filaments, *Curr. Opin. Cell Biol. 9*, 109−115.
59. Hofer, D., Ness, W., and Drenckhahn, D. (1997) Sorting of actin isoforms in chicken auditory hair cells, *J. Cell Sci. 110*, 765−770.
60. Herman, I. M. (1993) Actin isoforms, *Curr. Opin. Cell Biol. 5*, 48−55.
61. Hill, M. A., and Gunning, P. (1993) β and γ actin mRNAs are differentially located with myoblasts, *J. Cell Biol. 122*, 825−832.

62. Hoock, T. C., Newcomb, P. M., and Herman, I. M. (1991) β-Actin and its mRNA are localized at the plasma membrane and the regions of moving cytoplasm during the cellular response to injury, *J. Cell Biol. 112*, 653−664.
63. Micheva, K. D., Vallee, A., Beaulieu, C., Herman, I. M., and Leclerc, N. (1998) β-Actin is confined to structures having high capacity of remodeling in developing and adult rat cerebellum, *Eur. J. Neurosci. 10*, 3785−3798.
64. Rohatgi, R., Ma, L., Miki, H., Lopez, M., Kirchhausen, T., Takenawa, T., and Kirschner, M. W. (1999) The interaction between N-WASP and the Arp2/3 complex links Cdc42-dependent signals to actin assembly, *Cell 97*, 221−231.
65. Kelley, L. A., MacCallum, R. M., and Sternberg, M. J. E. (2000) Enhanced Genome Annotation using Structural Profiles in the Program 3D-PSSM, *J. Mol. Biol. 299*, 499−520.
66. Nakamura, F., Huang, L., Pestonjamasp, K., Luna, E. J., and Furthmayr, H. (1999) Regulation of F-actin binding to platelet moesin in vitro by both phosphorylation of threonine 558 and polyphosphatidylinositides, *Mol. Biol. Cell 10*, 2669−2685.
67. Martel, V., Racaud-Sultan, C., Dupe, S., Marie, C., Paulhe, F., Galmiche, A., Block, M. R., and Albiges-Rizo, C. (2001) Conformation, localization, and integrin binding of talin depends on its interactions with phosphoinositides, *J. Biol. Chem. 276*, 21217−21227.
68. McPherson, P. S. (2002) The endocytic machinery at an interface with the actin cytoskeleton: A dynamic, hip intersection, *Trends Cell Biol. 12*, 312−315.
69. Thompson, J. D., Higgins, D. G., and Gibson, T. J. (1994) CLUSTAL W: Improving the sensitivity of progressive multiple sequence alignment through sequence weighting, position-specific gap penalties and weight matrix choice, *Nucleic Acids Res. 22*, 4673−4680.

BI0487239